Molecular Catalysis xxx (xxxx) xxx–xxx

Contents lists available at ScienceDirect

Molecular Catalysis

journal homepage: www.elsevier.com/locate/mcat

Deactivation of Cu–Mg–Al mixed oxide catalysts for liquid transportation fuel synthesis from biomass-derived resources

P.J. Luggren, J.I. Di Cosimo*

Catalysis Science and Engineering Research Group (GICIC), INCAPE, UNL-CONICET, CCT CONICET Santa Fe, Colectora Ruta Nac. 168, km 0, Paraje "El Pozo", 3000 Santa Fe, Argentina

ARTICLE INFO

Keywords:
2-Hexanol
Aldol condensation
Cu-Mg-Al mixed oxides
Deactivation

ABSTRACT

A "platform molecule" (2-hexanol) obtained from the primary conversion of sugars was upgraded to liquid transportation fuel precursors under gas phase conditions at 573 K and 101.3 kPa. Reaction was promoted by Cu-Mg-Al mixed oxides with different copper loading (0.3–61.2%) and a Mg/Al = 1.5 (molar ratio). Products were mainly low oxygen content C9-C24 oxygenates and hydrocarbons. The product pool average molecular weight and the oxygenates/hydrocarbons ratio increase with the catalyst copper loading, but the latter might be diminished by augmenting the contact time. A slow catalyst deactivation process occurs in the first 2 h of reaction. Temperature-programmed oxidation, BET surface are measurements and X-ray photoelectron and Auger electron spectroscopies of the spent catalysts indicated that the main reasons for the activity decay during reaction are carbon deposition on the active sites and, to a lesser degree, partial oxidation of the surface copper particles. Oxygenates (reactant or products) are the chemical species responsible for deactivation. The initial deactivation rate (r_{d0}) depends on the copper content and contact time. On catalysts with low Cu content, r_{d0} is higher at short contact times, which is consistent with coke formed directly from the reactant. Contrarily, at high Cu loadings r_{d0} increases with contact time and parallels formation of heavy unsaturated oxygenates. Oxidation/reduction/catalytic test cycles of spent Cu-Mg-Al mixed oxides were implemented to explore catalyst reusability.

1. Introduction

In the last decade, biomass-derived renewablefeedstocks have been shown as potential resources for the production of biofuels; several strategies have been postulated for this purpose [1,2]. First-generation biofuels (biodiesel and bioethanol) are already commercially implemented in the transportation sector. However, in addition to technical limitations, these options consume edible resources (triglycerides and sucrose) and therefore, face ethical concerns derived from the competitive use of land for obtaining nonedible final products.

Recently, it has been discussed in the literature the use of lignocellulose, the most abundant carbohydrate in nature, as an inexpensive feedstock for second-generation liquid fuel production in a biorefinery [3–6]. Several procedures can be implemented in a biorefinery to treat and degrade lignocellulosic biomass. In particular, separation of sugars from lignin is attained by chemical or biological hydrolysis. Sugars, in turn, can be further converted into valuable chemicals and transportation fuels [5,7]. Scheme S1 of the Supplementary information file depicts the process from lignocellulose to liquid fuels.

Liquid transportation fuels are nonoxygenated hydrocarbons with different molecular weight range depending on the final application: C5-C12 for gasoline, C9-C16 for jet fuel and C12-C20 for diesel [1]. Thus, in order to be used in liquid fuel applications, sugars must be submitted to conversion strategies that include oxygen removal as well as carbon chain lengthening steps [1,8].

The primary conversion of sugars gives rise to the so called "platform molecules" comprising C4-C6 oxygenates such as secondary alcohols, ketones, furan-derivatives and acids [1,8,9], Scheme S1. In particular, 2-hexanol is obtained as the main constituent of the secondary C4-C6 alcohol fraction [10]. We recently reported the synthesis of liquid transportation fuel precursors on Cu-Mg-Al catalysts, at mild conditions and using 2-hexanol as a model "platform molecule" [11–13]. We showed that through a series of consecutive steps comprising dehydrogenation/C−C coupling/dehydration/hydrogenation reactions, high yields (≈90%) of C9-C24 oxygenates and hydrocarbons can be obtained. Most of the C9-C24 mixture is in the carbon atom range for jet fuel applications and contains a low O/C atomic ratio (≈0.025). We discussed also in those previous works that two main reaction pathways lead toward even or odd carbon atom number

* Corresponding author.
E-mail address: dicosimo@fiq.unl.edu.ar (J.I. Di Cosimo).

https://doi.org/10.1016/j.mcat.2018.08.008
Received 17 April 2018; Received in revised form 1 August 2018; Accepted 12 August 2018

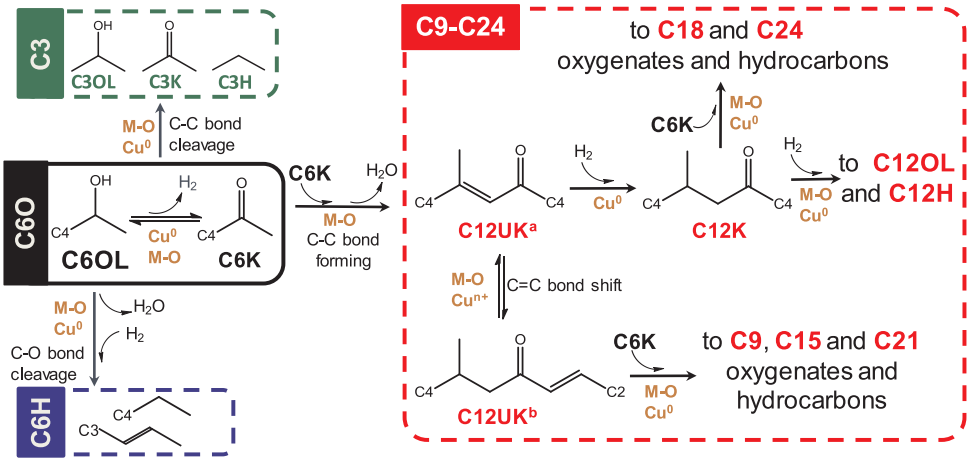

Scheme 1. Sequence of reactions involved in the C6OL conversion on ZCuMgAl catalysts [M-O: acid-base pair (M = Lewis acid cations, Mg^{2+} and Al^{3+}); CnO: Oxygenates; CnH: Hydrocarbons; CnOL: Alcohols; CnK: Saturated ketones; CnUK: Unsaturated ketones; n = 3, 6, 9, 12, 15, 18, 21 and 24 (carbon atom number)].

products and the operational conditions that favor one over the other. Scheme 1 presents a simplified version of the reaction pathways toward C9-C24 products from 2-hexanol. Furthermore, for the reactions promoted by Cu-Mg-Al oxides, we studied the chemical aspects of the active sites participating in kinetically relevant reaction steps and gave insight into the bifunctional Cu°/acid-base nature of the catalytic process; we concluded that the rate-limiting step (r.l.s.) and the corresponding active site shift as the Cu loading increases.

In this work we investigate the deactivation of the Cu-Mg-Al oxides during gas-phase 2-hexanol upgrading to liquid fuel precursors. The effect of the Cu content on the rate of deactivation was studied with a series of catalyst having between 0.3 and 61.2 wt.% Cu. Carbon deposition, metal particle sintering, changes in the copper oxidation state and modification of textural properties were analyzed as the possible causes of catalyst deactivation. Thus, temperature-programmed oxidation, BET surface are measurements and X-ray photoelectron and Auger electron spectroscopies were employed to analyze spent catalysts. Furthermore, changes of activity, selectivity and deactivation rate were investigated at different contact times and catalyst compositions with the purpose to identify the possible chemical species as well as other causes responsible for deactivation. The possibility of catalyst regeneration and reuse was also studied.

2. Experimental

2.1. Catalyst synthesis and characterization

Cu-Mg-Al precursors of the mixed oxides were prepared by co-precipitation of the metal nitrates with a KOH/K_2CO_3 solution at a constant pH of 10. Catalyst were prepared with a Mg/Al (atom ratio) of 1.5 and different Cu loadings. Details are given elsewhere [14]. After filtering, washing and drying at 363 K, precipitates were decomposed overnight in air at 773 K. The resulting mixed oxides were identified as ZCuMgAl, where Z is the copper content expressed in wt. % (Z = 0.3–61.2 wt. %). BET surface areas (*SA*) were measured by N_2 physisorption at 77 K in an Autosorb Quantachrome 1-C sorptometer. Powder X-Ray diffraction (XRD) technique was used to investigate the mixed oxide structural properties in a Shimadzu XD-D1 instrument. The average CuO crystallite size was calculated from the ($\bar{1}11$) diffraction line applying the Scherrer`s equation. The catalyst Cu chemical content was analyzed by Atomic Absorption Spectrometry (AAS).

The catalyst base site number (n_b, μmol/g catalyst) was measured by temperature-programmed desorption (TPD) of CO_2, as described in detail elsewhere [13].

Reduction of the copper phase was studied by temperature programmed reduction (TPR) using 5% H_2/Ar at a flow rate of 50 mL/min and at a heating rate of 10 K/min [15]. The quantitative hydrogen consumption was measured with a mass spectrometer (MS) in a Baltzers Omnistar unit. Previously, a calibration curve was constructed by reducing known amounts of pure CuO powder (Cicarelli, PA).

The dispersion of the metallic copper particles ($D = Cu^S / Cu^T_{AAS}$) was measured by a combination of TPR and N_2O decomposition techniques [16,17]. The amount of surface metallic copper species ($n_{Cu°}$, μmol Cu/g catalyst) and *D* were determined after sample reduction, followed by superficial re-oxidation of Cu° species to Cu_2O using N_2O ($2\,Cu° + N_2O \rightarrow Cu_2O + N_2$). Then, a TPR experiment was carried out to reduce the surface Cu_2O ($Cu_2O + H_2 \rightarrow 2Cu° + H_2O$). From the area under the TPR curve, the hydrogen uptake was determined and Cu^S in g Cu/g cat was calculated. Cu^T_{AAS} in g Cu/g cat is the total copper content in the catalyst formulation measured by AAS ($Cu^T_{AAS} = Z/100$). More details are given elsewhere [13].

Carbon deposits formed on the catalysts were characterized after reaction in a temperature-programmed oxidation (TPO) unit. The TPO experiments were carried out in a microreactor using 60 mL/min of a 2% O_2/N_2 oxidation gas mixture and a heating rate of 10 K/min; temperature was increased from room temperature to 1073 K. The reactor exit gases were fed into a methanator reactor loaded with a Ni/Kieselghur catalyst operating at 673 K. CO_x gases were thus converted into methane and then analyzed by a flame ionization detector. Quantitative results were obtained after calibration with known amounts of activated carbon (Carbonac G-160, 900 m^2/g). Deconvolution of the TPO signal was carried out using Gaussian functions.

The chemical nature of the surface species present on used catalysts was determined by Infrared Spectroscopy (IR). Fresh and used samples were analyzed in a Shimadzu FTIR Prestige-21 spectrophotometer. An inverted T-shaped cell containing the sample wafer and fitted with CaF_2 windows was used. The wafer of the sample diluted with KBr was evacuated at 573 K and then cooled down to room temperature to take the spectrum. Spectra of the species adsorbed on used samples were obtained by subtracting the fresh catalyst spectrum.

Surface species were analyzed by X-ray photoelectron spectroscopy (XPS) and Auger electron spectroscopy (XAES) using a multitechnique system (SPECS) equipped with a dual Mg/Al X-ray source and a hemispherical PHOIBOS 150 analyzer operating in the fixed analyzer transmission (FAT) mode. The spectra were recorded with the analyzer in constant pass-energy mode (pass energy at 30 eV) and with an Al Kα X-ray radiation source ($h\nu$ = 1486.6 eV). Before the XPS measurements, fresh samples were reduced in a 5% H_2/Ar flow at 573 K whereas used samples were heated up to 573 K in an Ar flow inside the pre-chamber. Samples were subsequently evacuated in ultra-high vacuum for at least two hours before reading. The data treatment was performed with the

Casa XPS program (Casa Software Ltd., UK) and the C1s peak position set at 284.6 eV was used as internal reference to locate the other peaks. The XPS peaks were fitted using the least-squares method and Gaussian (70%)-Lorentzian (30%) peak shapes.

2.2. Catalytic testing

The conversion of 2-hexanol (C6OL) was studied in the gas phase at 573 K and 101.3 kPa in a fixed-bed reactor. Catalysts were pretreated in situ in a flow of N_2 at 773 K for 1 h and then reduced in flowing H_2 (35 mL/min) at 573 K for 1 h before the catalytic test. C6OL (Aldrich ≥ 98.0%) was introduced via a syringe pump and vaporized into flowing N_2 or H_2 to give a pressure ($\overline{P}_{C6OL}$) of 4.1 kPa. On-line analysis of the reaction products was carried out by gas chromatography using an Shimadzu GC-2014 chromatograph equipped with flame ionization detector and a (5% Phenyl)-methylpolysiloxane HP-5 Agilent capillary column. More details are given elsewhere [11]. Main products were coded as CnH (hydrocarbons), CnK (saturated ketones), CnUK (unsaturated ketones) and CnOL (alcohols), where n stands for the carbon atom number in the molecule (n = 3, 6, 9, 12, 15, 18, 21 and 24). CnO is the code for oxygenate products (other than the reactant pool). Because of the equilibrated nature of C6OL-C6K interconversions [18] these two molecules were assumed hereinafter as the reactant pool (C6O = C6OL + C6K). Thus, conversion was defined as:

$$X_{C6O} = \left(1 - \frac{F_{C6OL} + F_{C6K}}{F^0_{C6OL}}\right)$$

where F_{C6OL} *and* F_{C6K} are the molar flow rate of C6OL and C6K, respectively, at the reactor exit; F^0_{C6OL} is the molar flow rate of C6OL in the reactor feed. Product selectivity was calculated on a carbon atom basis, as:

$$S_i = \frac{F_i n_i}{\Sigma F_i n_i}$$

where F_i and n_i are the flow rate and the carbon atom number of product "i", respectively. Relative concentrations are defined as:

$$C_i = \frac{F_i n_i}{F^0_{C6OL}\, n_{C6OL}}$$

For products, C_i coincides with the yield whereas for the reactant pool $C_{C6O} = 1\text{-}X_{C6O}$.

Carbon balances closed to within 90–98%. Contact times (W/F^0_{C6OL}) were varied in the range of 6–350 g catalyst h mol of $C6OL^{-1}$ (W is the catalyst loading).

3. Results and discussion

3.1. Characterization of the ZCuMgAl mixed oxides

A set of ZCuMgAl (Z = 0.3–61.2 wt.% Cu) mixed oxides having a Mg/Al = 1.5 (molar ratio) was prepared. These catalysts combine a metallic function provided by Cu° atoms and acid-base sites (M–O pairs; M: Mg^{2+} and Al^{3+}). A detailed characterization of these materials was reported in previous works [11,13]. A summary of the main physicochemical properties of the ZCuMgAl oxides is given in Table 1.

Surface area (*SA*) values were rather constant for samples with Cu loadings Z ≤ 15.1 wt.% but decreased at higher Z because the Al content also decreased. Aluminum is known to be a textural promoter that stabilizes the porous structure and the copper particles [19,20].

A quasi-amorphous MgO (periclase, ASTM 4-0829) phase was detected by XRD in the low copper content ZCuMgAl oxides (Z < 15.1 wt.%). At higher Z values an incipient CuO (tenorite, ASTM 5-0661) phase was observed which became the only detectable phase at Z = 62.1 wt.% Cu.

ZCuMgAl oxides with Z ≥ 4.1 wt.% can be completely reduced at temperatures below 653 K [13]; in Table 1, T_M indicates the temperature at peak maximum of the TPR experiments. For these materials, the Cu° dispersion (*D*) was calculated by combining TPR and N_2O decomposition experiments as described in section **2.1.** The results obtained (Table 1) are in line with values reported in the literature for similar Cu-based oxides [21–24]. The amount of exposed Cu° species on the surface in μmol Cu°/g cat ($n_{Cu^\circ} = 157 \times D \times Z$) was also calculated, Table 1; the n_{Cu° values increased with increasing Z despite of the fact that *D* decreased. Thus, at high Cu contents the ZCuMgAl oxides contain more but larger Cu° domains on the surface. For ZCuMgAl oxides with Z < 4.1 wt.% meaningful *D* values could not be measured because of two reasons: incomplete sample reduction even at 850 K [13] and operational limitations to carry out the quantitative TPR experiment under conditions free of artifacts [25].

The surface basic properties of the ZCuMgAl oxides were investigated by TPD of CO_2. The total number of base sites (n_b, μmol/g cat) was calculated by integration of the TPD curves (not shown here). Table 1 shows that the n_b values decreased as Z increased. Furthermore, in a previous work we discussed that the overall base site strength of the ZCuMgAl oxides is enhanced at low Z values and decreases at high Cu loadings as a consequence of the decreasing Mg content [13].

In summary, the ZCuMgAl samples contain surface Cu° species and acid-base sites with mainly basic properties and the contribution of each of them after reduction strongly depends on the oxide composition.

3.2. Catalytic activity

The set of ZCuMgAl catalysts with different copper contents (Z = 0.3, 0.6, 1.2, 1.8, 4.1, 8.0, 15.1, 32.7 and 61.2 wt.% Cu) were tested in the gas phase conversion of 2-hexanol (C6OL) at 573 K A detailed discussion of the catalytic results was reported recently [13]. Several reaction pathways take place on ZCuMgAl catalysts as depicted in Scheme 1 . Quantified products contain carbon atom numbers in the range of n = 3–24 (C3–C24) and can be grouped in three categories: C3 compounds, C6H hydrocarbons and heavier C9-C24 compounds. The latter are the compounds of interest since they are jet and diesel fuel precursors. The C9-C24 products are branched hydrocarbons, ketones and alcohols. Scheme 1 also shows the two different pathways leading to odd (C9, C15 and C21) and even (C12, C18 and C24) carbon atom number compounds.

Formation of short chain C3 compounds by C—C bond cleavage and of C6 hydrocarbons (hexene/hexane, C6H) by dehydration/hydrogenation is undesirable for liquid transportation fuel purposes. The pathway toward liquid fuel precursors starts by the dehydrogenation of C6OL to C6K. Then, one or several C—C bond forming aldol condensation reactions occur as part of the sequence of consecutive reaction steps that comprises dehydrogenation, C—C coupling, dehydration and hydrogenation reactions.

Also, the bifunctional Cu°/acid-base nature of the catalytic process was discussed earlier for ZCuMgAl oxides and other similar catalysts [11,13]. We demonstrated that both, the rate-limiting step (r.l.s.) and the corresponding active site, change as the n_b/n_{Cu° ratio becomes progressively larger, i.e., as the Cu loading decreases. Thus, on catalysts with $n_b/n_{Cu^\circ} \leq 3$ (high Z values) a base-catalyzed reaction step is rate limiting, i.e., a C—C bond forming step. Contrarily, on catalysts with enhanced basic properties ($n_b/n_{Cu^\circ} > 3$), which are difficult to reduce [13], the catalytic process is limited by one of the Cu°-promoted hydrogenation steps.

Fig. 1 compares the time on stream (t.o.s.) performance of selected ZCuMgAl catalysts (Z = 0.6, 8.0 and 32.7 wt. % Cu) for a reactant pool conversion of ~20% measured at t = 0 ($X_{C6O_{t=0}}$). The whole set of samples was tested at similar conversion levels and samples of Fig. 1 were chosen to represent low, intermediate and high Cu content catalysts. A logarithmic scale was used to highlight the time evolution of X_{C6O} and selectivity to main products (S_{Cn}). Cn products (n = 3, 6, 9, 12, 15, 18, 21 and 24) were plotted without discrimination between

Table 1
Physicochemical properties of fresh ZCuMgAl catalysts.

Catalyst	Nominal Composition		Surface area, *SA* (m^2/g)	Pore volume (cm^3/g)	Structural analysis by XRD	Metallic (Cu°) and basic properties				
	Z (wt.% Cu)	Mg/Cu (molar)			Phases detected	D[a] (%)	n_{Cu°[b] (μmol/g)	T_M[c]	n_b[d] (μmol/g)	n_b/n_{Cu°
0.3CuMgAl	0.5	172.97	226	0.318	MgO	–	–	–	527	
0.6CuMgAl	0.8	106.83	218	0.405	MgO	–	–	–	532	
1.2CuMgAl	1.0	85.46	294	0.476	MgO	–	–	681	511	
1.8CuMgAl	2.0	42.08	225	0.324	MgO	–	–	658	497	
4.1CuMgAl	4.2	19.54	223	0.394	MgO	16.9	109	586	413	3.79
8.0CuMgAl	10.0	7.58	248	0.399	MgO	12.2	153	571	457	2.96
15.1CuMgAl	15.0	4.69	208	0.266	MgO-CuO	10.2	243	539	412	1.70
32.7CuMgAl	35.0	1.39	90	0.172	MgO-CuO	5.6	287	506	225	0.78
61.2CuMgAl	70.0	0.15	42	0.087	CuO	4.4	421	493	66	0.16

[a] Cu° dispersion by N_2O decomposition.
[b] number of exposed Cu° atoms.
[c] Temperature at peak maximum by TPR.
[d] base site number by TPD of CO_2.

hydrocarbons (CnH) and oxygenates (CnO). A decay of X_{C6O} was observed at the beginning of the reaction, which could be assigned to a catalyst deactivation process. After 1.5 h of t.o.s. X_{C6O} reached a rather constant value whereas selectivities still evolved with time.

Fig. 1 also shows that on 0.6CuMgAl the main constituents of the C9-C24 fraction were C12 compounds whereas on 8.0CuMgAl and 32.7CuMgAl, odd (C9, C15 and C21) and heavier even (C18 and C24) products were found in addition to C12. The results on 0.6CuMgAl were explained by the fact that after C12 formation, the surface of low Z catalysts (low number of surface Cu° species) is deprived of the necessary hydrogen fragments to keep the aldol condensation sequence going and therefore, the C−C bond formation stops after the first aldolization reaction. Moreover, in that compositional range, the unreduced Cu^{n+} species contribute to promote, together with the acid-base sites, the C=C bond shift of the C12UK[a] intermediate, which enables the pathway toward odd carbon atom number compound formation (Scheme 1).

Due to the catalyst deactivation process, the catalytic results obtained with all the ZCuMgAl catalysts were compared at similar conditions (at t = 0). The results at t = 0 were calculated by extrapolation of the reactant conversion and product selectivity curves to zero time on stream. Fig. 2A summarizes the effect of varying Z on the product selectivity at t = 0 ($S_{Cn_{t=0}}$) for the whole set of ZCuMgAl catalysts. Products were grouped and color-coded as in Scheme 1 . The C9–C24 group was broken down into two groups to show the contribution of jet (C9–C15) and diesel (C18–C24) fuel precursors. The product distribution depended on the copper content, but regardless of the catalyst composition, most of the products were C9–C15 compounds. The $S_{C9-C24_{t=0}}$ slightly increased with Z from 80% to 92% mainly because of the enhanced contribution of the C18–C24 fraction at high copper loadings. This result indicates that the latter are preferentially promoted on catalysts with a low n_b/n_{Cu° ratio on which the numerous surface Cu° species activate the O−H bond of C6OL in the initial dehydrogenation reaction step, favoring the pathway toward the aldol condensation sequence. Although $S_{C3_{t=0}}$ was negligible on all the ZCuMgAl catalysts, it seems that the C−C bond cleavage is promoted on the abundant surface Cu° species of low n_b/n_{Cu° catalysts. Contrarily, the C6OL dehydration (C−O bond cleavage) toward C6H compounds is likely to occur on low copper content catalysts, which are hard to reduce and therefore, their surfaces preferentially contain acid-base sites and a low number Cu° species.

Fig. 2B shows at t = 0 how the oxygenate fraction increases with Z and the resulting decrease of the hydrocarbon selectivity. Also, calculations of the average molecular weight of the C3–C24 products suggest that the higher the copper loading, the heavier the products formed.

In addition to the experiments of Figs. 1 and 2, selected ZCuMgAl catalysts (Z = 0.6, 8.0 and 32.7 wt.% Cu) were catalytically tested at higher conversions. Thus, the contact time (W/F^0_{C6OL}) was varied in a wide range to reach, in some cases, near 100% conversions. Fig. S1 of the Supplementary information file shows the t.o.s. performance of the three catalysts at the highest W/F^0_{C6OL} tested; conversion and selectivities to main products reached steady values after 2 h of t.o.s. Similar conclusions were obtained from an extended additional experiment carried out for 12 h with sample 8.0CuMgAl at W/F^0_{C6OL} = 100 gh/mol ($X_{C6O_{t=0}}$ ~50%), Fig. S2. By extrapolation of the conversion and selectivity curves to zero t.o.s., the $S_{Cn_{t=0}}$ (C3, C6H and C9–C24 products) and conversions ($X_{C6O_{t=0}}$) were calculated at t = 0 for the three catalysts. C9–C24 products, with diesel and jet fuel applications, were obtained with more than 73% selectivity whereas $S_{C3_{t=0}}$ was always lower than 5% on the three catalysts. On the other hand, low (0.6CuMgAl)

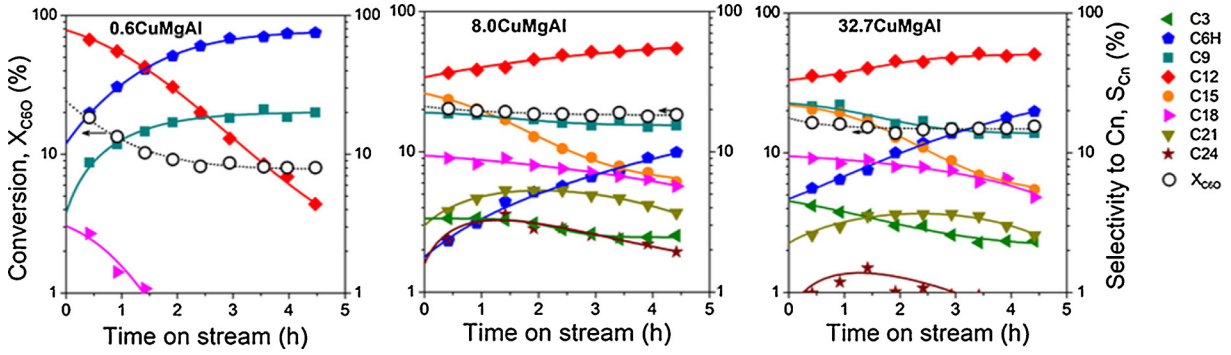

Fig. 1. Conversion and selectivity to main products as a function of time on stream for selected ZCuMgAl catalysts [Z= 0.6, 8.0 and 32.7 wt.% Cu; T = 573 K; P = 101.3 kPa; $\overline{P}_{C6OL}$ = 4.1 kPa; N_2 balance; $X_{C6O_{t=0}}$ ~20%; n: number of carbon atoms].

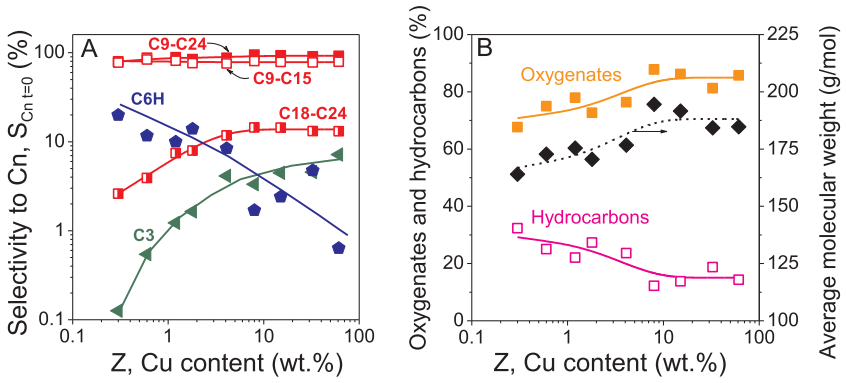

Fig. 2. Effect of the copper content on the product quality at t = 0. (A) Selectivity to main products; (B) Selectivity to oxygenates and hydrocarbons and average molecular weight of products [t = 0; T = 573 K; P = 101.3 kPa; $\overline{P}_{C6OL}$ = 4.1 kPa; N_2 balance; $X_{C6O_{t=0}}$ ~20%; n: number of carbon atoms].

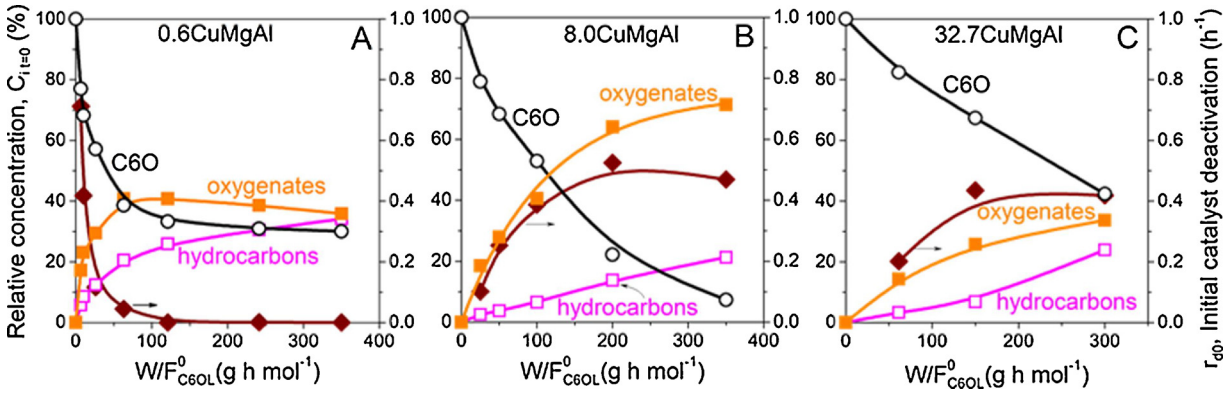

Fig. 3. Relative concentration of products and reactant pool, and initial deactivation rate at different contact times (W/F^0_{C6OL}) for selected ZCuMgAl catalysts. (A) 0.6CuMgAl; (B) 8.0CuMgAl; (C) 32.7CuMgAl [t = 0; T = 573 K; P = 101.3 kPa; $\overline{P}_{C6OL}$ = 4.1 kPa; N_2 balance].

and high (32.7CuMgAl) copper content catalysts produced significant amounts of C6H (13–22%) at high conversions. Fig. 3 summarizes the results at different W/F^0_{C6OL} and at t = 0 on the three catalysts. Results are expressed in terms of relative concentrations, $C_{i_{t=0}}$(%), of products (C3–C24 oxygenates and hydrocarbons) and reactant pool (C6O). Conversion can be easily calculated from the relative concentration of the reactant pool as $X_{C6O_{t=0}}$(%) = 100−$C_{C6O_{t=0}}$(%). Sample 32.7CuMgAl was less active than the others and the highest $X_{C6O_{t=0}}$ with this catalyst was 58% at W/F^0_{C6OL} = 300 gh/mol, whereas 8.0CuMgAl and 0.6CuMgAl reached 93% and 70%, respectively, at W/F^0_{C6OL} = 350 gh/mol. According to the shape of the product curves, oxygenates are primary products formed in the initial stages of the reaction, whereas hydrocarbons are secondary products formed from the latter, as postulated in Scheme 1 . Moreover, regardless of the composition or contact time, oxygenates are the predominant products even at high conversions.

3.3. Catalyst deactivation

There are many factors that can affect the catalyst stability during dehydrogenation/aldol condensation/dehydration/hydrogenation reactions such as water formation, sintering of the copper particles and coke deposition. Water produced in dehydration and C−C bond forming steps (Scheme 1) might modify the base site strength by converting strong surface O^{2-} species in weak OH- groups. However, at the reaction conditions of this work (573 K), the surface partial pressure of water should be negligible and therefore, the influence of water could probably be ruled out. We reached similar conclusions in a previous work on aldol condensation of acetone on MgO [26]. On the other hand, sintering of the Cu° particles caused by hydrogen build-up during reaction (dehydrogenation of C6OL) is not likely to contribute to the deactivation process because the catalysts are reduced with pure hydrogen at 573 K before the catalytic tests at the same temperature. However, changes in the oxidation state of the copper particles during reaction cannot be disregarded.

The textural properties of selected ZCuMgAl catalysts (Table 2) were compared after testing them at similar reaction conditions (573 K and $X_{C6O_{t=0}}$ ~50%). A surface area decline, compared to their fresh homologues of Table 1, is evident. This result can be explained by partial pore blocking caused by deposition of carbonaceous residues. As discussed above, we detect in the gas phase oxygenates and hydrocarbons of up to 24 carbon atoms. These or heavier high boiling point compounds are likely to irreversibly adsorb on the catalyst surface

Table 2
Characterization of used ZCuMgAl catalysts.

Catalyst	Surface area, *SA*[a] (m^2/g)	Pore volume[a] (cm^3/g)	TPO analysis[b]				
			Carbon content (wt.%)	l.t.p. (K)	l.t.p. (area%)	h.t.p. (K)	h.t.p. (area%)
0.3CuMgAl	n/d	n/d	4.1	597	19.5	670	80.5
0.6CuMgAl	167	0.257	3.7	597	19.6	681	80.4
1.2CuMgAl	n/d	n/d	5.2	596	19.5	682	80.5
1.8CuMgAl	n/d	n/d	5.1	599	24.1	646	75.9
4.1CuMgAl	n/d	n/d	6.7	579	24.4	639	75.6
8.0CuMgAl	193	0.339	8.9	554	25.6	619	74.4
15.1CuMgAl	n/d	n/d	6.3	555	27.9	610	72.1
32.7CuMgAl	59	0.177	5.2	525	44.1	607	55.9
61.2CuMgAl	n/d	n/d	1.5	522	57.4	610	42.6

[a] after catalytic runs at $X_{C6O_{t=0}}$ ~50%.
[b] after catalytic runs at $X_{C6O_{t=0}}$ ~20%; n/d: not determined; l.t.p.: low temperature peak; h.t.p.: high temperature peak.

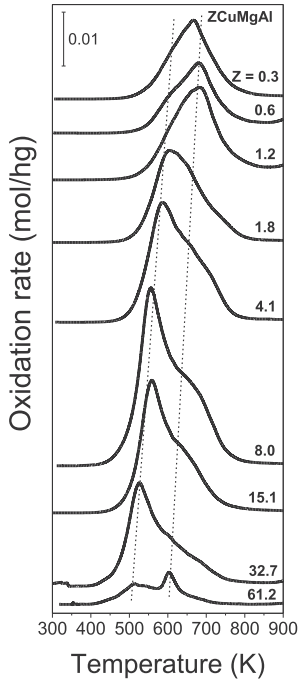

Fig. 4. TPO of ZCuMgAl catalysts after catalytic testing. Reaction conditions as in Fig. 2.

causing both, activity and surface area decay. Moreover, in some cases the coke precursors may be formed from the reactant pool, as will be discussed below.

3.3.1. Coke formation and characterization

Time ago, during the study of the gas-phase acetone oligomerization on MgO and Mg-Al mixed oxides we found that catalysts deactivate during reaction because of coke formation (carbon deposits) that blocks pores and surface base sites [26,27]. We concluded that coke precursor species were unsaturated oxygenates (formed by aldol condensation-like reactions). Both, in the previous works and here, these compounds were not detected in the gas phase analysis during reaction because they remain bound to the surface due to the strong interaction between the unsaturated chain and the active sites. Thus, taking into account the different unsaturated compounds and aldol condensation steps that participate in the reaction sequence of Scheme 1, we investigated here by TPO the possible presence of carbon deposits on the catalysts after the catalytic runs. Fig. 4 and Table 2 summarize the oxidation results carried out after the catalytic experiments of Fig. 2, i.e, at $X_{C6O_{t=0}}$ ~20%. The amount of carbon measured on the ZCuMgAl catalysts was between 1.5 and 8.9 wt.% with no clear dependence on the copper content. The TPO curves of Fig. 4 show the existence of two different carbon deposits: a low temperature peak (l.t.p.) centered at 520–600 K and a high temperature peak (h.t.p.) at 610–680 K. Thus, the TPO traces were deconvoluted in two peaks and the quantitative results are presented in Table 2.

Both kind of carbon residues seem to be related to the metallic and acid-base properties of the ZCuMgAl catalysts since as shown in Table 2, the contribution of the l.t.p. and h.t.p (in area %) depends on Z. Furthermore, both peak maxima shift to lower temperatures with increasing Z. Thus, on catalysts with a high copper content (catalysts with significant n_{Cu° values, Table 1) the carbonaceous residues are oxidized at lower temperatures. This can be explained considering that the l.t.p. corresponds to coke deposited on Cu° sites and that those metallic species participate in the catalytic coke oxidation process during TPO experiments. At low Z values (catalysts with predominant basic properties and high n_b values, Table 1) the contribution of the h.t.p. is notoriously enhanced at the expense of the l.t.p. As explained above, in these materials copper is diluted and buried inside the mixed oxide matrix making the catalyst reduction difficult under standard conditions [13]; coke therefore forms mainly on the abundant basic sites giving rise to the h.t.p. The shift of the latter to lower temperatures at higher copper loadings might be ascribed to a catalytic effect of the increasing amounts of the vicinal Cu° sites. These sites generate surface oxygen fragments that promote the oxidation of those carbonaceous species at lower temperature.

The assignment of the h.t.p. to carbon deposits on basic sites and of the l.t.p. to those formed on Cu° sites is supported by additional TPO experiments carried out on reference materials. In a previous work [11] we tested in the same reaction several single oxides such as MgO and Al_2O_3, and mixed oxides (Cu-Mg and Cu-Al) prepared by coprecipitation such as 9.8CuMg (9.8 wt.%Cu) and 6.4CuAl (6.4 wt.% Cu). The TPO results of those samples after reaction are shown in Fig. S3 of the Supplementary information file. Clearly, the figure shows that the catalyst acid-base and metallic properties play a role on the nature of the carbon deposits. Coke formed on acidic Al_2O_3 (h.t.p. at 750 K) is more difficult to remove by oxidation than that on basic MgO (peak at 644 K). Similar findings were reported previously for the coke formed on MgO and Mg-Al mixed oxides tested in the acetone aldol condensation [27]. Thus, for low copper loadings ZCuMgAl catalysts, in which the influence of the Cu° species on the oxidation temperature is almost negligible, the combination of Mg^{2+} and Al^{3+} cations in a Mg/Al = 1.5 (molar ratio) explains the position of the h.t.p. in Fig. 4 at ~680 K. Furthermore, Fig. S3 confirms that the effect of copper inclusion in the catalyst formulation (samples 9.8CuMg and 6.4CuAl), is the shift of the peak positions to lower oxidation temperatures compared to the single oxides and the appearance of a second peak at lower temperatures in the case of 9.8CuMg. Fig. S3 also suggests that the presence of Cu° species in the catalyst decreases the final carbon content.

3.3.2. Deactivation causes, quantification and dependence on the experimental variables

In order to get insight into the reasons and species responsible for catalyst deactivation, a quantification of the phenomenon was intended by defining the relative catalytic activity as in Eq. (1):

$$a_{(t)} = \frac{r_t}{r_0} \tag{1}$$

where r_t and r_0 are the reaction rates at t.o.s. t and 0, respectively. The deactivation rate was then defined as indicated in Eq. (2):

$$r_d = -\frac{da}{dt} \tag{2}$$

The deactivation rate is usually expressed in terms of a power-law dependence of the activity, where m is the deactivation order, $k_{d(T)}$ is the deactivation rate constant and $\varnothing_{(Ci)}$ is a function of the concentration of the gas phase compounds, Eq. (3) [28,29].

$$r_d = k_{d(T)} \varnothing_{(Ci)} a^m \tag{3}$$

An expression of r_d as a function of the relative concentrations of reactants and products causing deactivation was postulated based on the simplified deactivation network depicted in Scheme 2 , Eq. (4). Thus, Eq. (4) takes into account the participation in the deactivation process of the reactant pool as well as of the oxygenate products. Moreover, in Eq. (4), k_{d3} represents the so called “independent deactivation”, i.e., a deactivation process unaffected by the concentration of

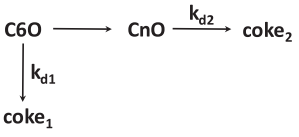

Scheme 2. Simplified deactivation reaction network for ZCuMgAl catalysts.

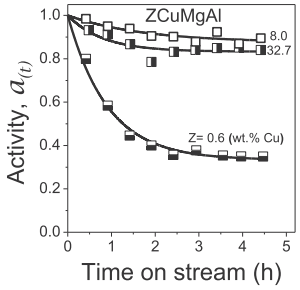

Fig. 5. Relative activity as a function of time on stream for ZCuMgAl catalysts [Z = 0.6, 8.0 and 32.7 wt.% Cu; T = 573 K; P = 101.3 kPa; $\overline{P}_{C6OL}$ = 4.1 kPa; N_2 balance; $X_{C6O_{t=0}}$ ~20%].

gas phase compounds, such as structural modifications, sintering or oxidation state change, among others [28].

$$r_d = [k_{d1} C^p_{C6O} + k_{d2} C^q_{CnO} + k_{d3}]\, a^m \quad (4)$$

From the conversion versus t.o.s. curves r_t and r_0 were calculated at different conditions. As an example, Fig. 5 shows the resulting activity decay for the experiments of Fig. 1 at $X_{C6O_{t=0}}$ ~20%. From the slopes of the curves of Fig. 5, the initial deactivation rate (r_{d0}) was calculated as in Eq. (5):

$$r_{d0} = \left[\frac{da}{dt}\right]_{t=0} \quad (5)$$

As can be seen in Fig. 5, the magnitude of the deactivation process depends on the catalyst composition. When comparing the three catalysts of Fig. 5, the highest initial deactivation rate was measured on sample 0.6CuMgAl (0.712 h^{-1}), whereas sample 8.0CuMgAl showed almost negligible deactivation (0.071 h^{-1}) and sample 32.7CuMgAl presented an intermediate value (0.201 h^{-1}); the high r_{d0} value of the former is probably due to the strongest basic properties of this sample [13] and to the fact that the strong sites are more susceptible to deactivate in the early stages of reaction. Similar calculations of r_{d0} performed on the complete set of ZCuMgAl catalysts tested at $X_{C6O_{t=0}}$ ~20% were plotted as a function of Z in Fig. 6. An explanation for the resulting inverted volcano curve is that the surface of low copper content ZCuMgAl catalysts contains mainly acid-base sites with predominant basic properties as well as hardly reducible copper species (Table 1); conversion of C6OL into C6K (Scheme 1) by dehydrogenation is not complete and therefore, the concomitant formation of hydrogen species required in the following aldol condensation steps is severely limited. As a consequence, the low pressure of surface-generated C6K restricts the extent of the pathway toward the consecutive C—C bond forming steps. Thus, deposition on the basic sites of the C6O reactant pool (C6OL and C6K) and light products formed directly from it, is likely to cause deactivation. In fact, Fig. 2A shows that low Z catalysts

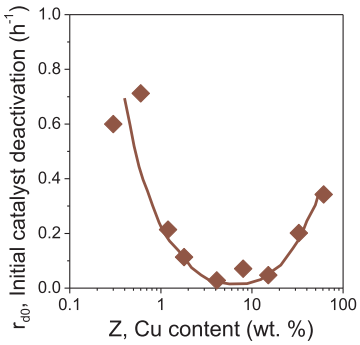

Fig. 6. Initial catalyst deactivation rate as a function of the copper content for ZCuMgAl catalysts [T = 573 K; P = 101.3 kPa; $\overline{P}_{C6OL}$ = 4.1 kPa; N_2 balance; $X_{C6O_{t=0}}$ ~20%].

produce C6H in significant amounts at t = 0, i.e., hexene and oligomerization products formed from it probably take part in the deactivation process. Thus, low copper content catalysts present high r_{d0} values. Similar findings were reported by Bravo et al [30] for the methanol/ethanol coupling on Cu-Mg-Al oxides; they associated the tendency of low-copper loading oxides to more strongly adsorb oxygenates to the higher temperature needed to reduce such materials. In agreement with that, Table 1 shows that our low Z value materials indeed reduce at higher temperatures (high T_M values); as explained in section **3.1**, for sample 0.6CuMgAl complete reduction could not be achieved at even 850 K.

On the other hand, on ZCuMgAl catalysts with a higher copper content (Z = 1.8–4.1 wt.% Cu) a proper combination of surface Cu° and acid-base sites generates a high concentration of surface hydrogen fragments (derived from the complete C6OL dehydrogenation) that readily reduce the unsaturated oxygenate products formed by aldol condensation steps. Consequently, the oxygenate/surface interaction decreases, as previously found in other aldol condensation reactions on similar catalysts [14]. In other words, hydrogenation of C=O or C=C bonds favors the product release to the gas phase as less unsaturated oxygenates or hydrocarbons and causes the notorious decrease of the r_{d0} values. Finally, on catalysts with Z ≥ 8.0 wt.% Cu, formation of heavier compounds (C18-C24, Fig. 2A) by sequential aldol condensation steps is enhanced. The surface hydrogen species formed by the initial C6OL dehydrogenation are probably not enough to reduce the many unsaturations of those heavy oxygenate intermediates that therefore would remain strongly bound to the surface causing deactivation (high r_{d0} values). The increasing contribution of oxygenates at high copper contents can be seen in Fig. 2B. Furthermore, on these samples the number of base sites (n_b) is drastically reduced (Table 1) whereas the probabilities of blocking these sites with oxygenates heighten.

After the analysis at low conversions ($X_{C6O_{t=0}}$ ~20%) and in an attempt to identify the species causing deactivation, the catalytic tests at different contact times (Fig. 3) were studied in more detail. Thus, the deactivation process was investigated at t = 0 and high conversions. At t = 0, $a_{(t)}$ = 1 and the initial deactivation rate (r_{d0}) from Eq. (4) becomes

$$r_{d0} = [k_{d1} C^p_{C6O_{t=0}} + k_{d2} C^q_{CnO_{t=0}} + k_{d3}] \quad (6)$$

From the conversion versus t.o.s. curves of the experiments of Fig. 3, the relative catalytic activity $a_{(t)}$ was calculated for selected ZCuMgAl catalysts (Z = 0.6, 8.0 and 32.7 wt.% Cu) at different t.o.s. and W/F^0_{C6OL} values. Fig. 7 shows the results of $a_{(t)}$ versus t.o.s. for sample 0.6CuMgAl showing that the catalyst activity decay diminishes with increasing W/F^0_{C6OL}, so that the deactivation was almost negligible at W/F^0_{C6OL} ≥100 gh/mol. The quantification of the deactivation process can be observed in Fig. 3A where the corresponding r_{d0} values were plotted versus W/F^0_{C6OL} (solid diamonds). Clearly, the r_{d0} curve follows a trend similar to that of the C6O curve thereby suggesting that deactivation is mainly caused by the reactant pool, as discussed above and as predicted by the first term of Eq. (6). This was confirmed by IR analysis

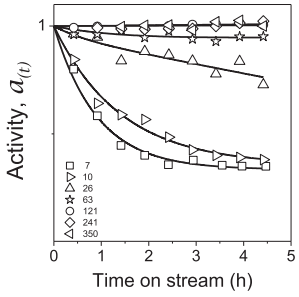

Fig. 7. Relative activity as a function of time on stream at different contact times (W/F^0_{C6OL}) for catalyst 0.6CuMgAl [W/F^0_{C6OL} in g h mol^{-1}; T = 573 K; P = 101.3 kPa; $\overline{P}_{C6OL}$ = 4.1 kPa; N_2 balance].

of used sample 0.6CuMgAl, Fig. S4. The bands at 1572-1540 and 1439, as well as the shoulder at 1384 cm^{-1} are typical features of the reactant pool adsorption. In fact, Jobson et al reported identical spectra for the desorption of 1-hexanol/1-hexanal at 478 K on Cu/Al_2O_3 [31]. At the highest conversion, C9-C12 are the main constituents of the oxygenate fraction ($S_{C9-C12_{t=0}}$~ 26%). Thus, after C12 formation consecutive aldol condensation steps do not proceed further, even at high conversions.

Similar calculations of $a_{(t)}$ and r_{d0} were performed for the other two samples with higher Z values and the r_{d0} results are shown in Fig. 3B and C as solid diamonds. For these samples r_{d0} increases with W/F^0_{C6OL} and the curve shape is similar to that of the oxygenate products. Thus, the increasing contribution of heavy oxygenates at high conversions is likely to be responsible for the catalyst deactivation, in agreement with what predicted by the second term of Eq. (6). In fact, at the highest conversion, heavy oxygenates (C9-C24) represent ~74% of the total products on sample 8.0CuMgAl and ~54% on sample 32.7CuMgAl. The attribution of catalyst deactivation on these samples to heavy oxygenates was corroborated by carrying out additional catalytic experiments in which 8.0CuMgAl was tested at 573 K and at different W/F^0_{C6OL} values but diluting C6OL in a hydrogen flow, Fig. S5. In the presence of molecular H_2 the role of oxygenates as intermediates is noteworthy since their hydrogenation to hydrocarbons takes place at shorter contact times compared to the results in N_2 (Fig. 3B). Thus, the oxygenate curve shows a clear maximum whereas that of hydrocarbons presents the sigmoidal shape typical of secondary products. The r_{d0} versus W/F^0_{C6OL} curve (solid diamonds in Fig. S5) obtained in H_2 parallels that of oxygenates, showing significantly lower values at high conversions where the concentration of oxygenates decreases. Indeed, at the highest conversion value ($X_{C6O_{t=0}}$~ 100%, W/F^0_{C6OL} = 150 gh/mol) the C9-C24 oxygenate fraction represents just 14% of the total products.

Additional experiments were made to confirm the presence of oxygenates on the surface of used samples and therefore, a XPS analysis on selected samples (Z = 0.6, 8.0 and 32.7 wt.% Cu) was performed. The surface of these three samples was compared after testing them at similar conditions ($X_{C6O_{t=0}}$~ 50%). Elements were measured in the C1s, O1s, Cu2p and Mg2p regions of the spectra. The XPS spectra of the C1s and O1s regions are presented in Fig. 8A and B, respectively. Fresh samples after in situ reduction at 573 K are shown in curves (a), (b) and (c), whereas used samples correspond to curves (d), (e) and (f). Compared to fresh samples, results of used catalysts in the C1s region (Fig. 8A) show an intensity increase of the adventitious carbon signal (C—C at 284.6 eV) and the development of new bands at higher binding energies (B.E.). In particular, used sample 8.0CuMgAl (curve (e), Fig. 8A) showed the largest C1s peak signal, in agreement with the TPO results. The C1s signal of used samples was deconvoluted in three peaks at 284.6, ~287.1 and ~289.2 eV. The bands at higher B.E. are compatible with organic carbon-oxygen species (C═O at 287.0–288.0 eV) probably superimposed to carbonate bands (289.0–291.5 eV) [32–34]. The peak at 287.1 eV, representing 3–10% of the total C1s peak area, was assigned to ketones and other oxygenates strongly bound to the surface after reaction. Thus, after the catalytic tests, the existence of oxygen-containing carbon deposits was confirmed. In agreement with those results, Fig. 8B shows broad asymmetric O1s bands in used samples attributed to the presence of organic oxygen species (C═O) at ~533.0 eV in addition to the mixed oxide signal at ~530.0 eV and carbonates at ~531.4 eV [35,36].

The surface atomic Cu/Mg ratio calculated using the 2p regions of the spectra showed similar values for fresh and used samples thereby indicating that no sintering of the copper particles has occurred during the catalytic tests. However, a closer inspection of the Cu spectra showed a change of the copper oxidation state after reaction, as will be discussed below.

It is well known that reliable discrimination between Cu^{1+} and Cu° species using the strong Cu XPS signals in the 2p regions is not possible. Therefore, a combination of Cu 2p XPS and Cu LMM Auger lines was used to assign the various copper oxidation states in freshly reduced and in used samples. The method suggested by Moretti based on the employ of the Warner plot and the calculation of the Auger parameter was used [37], as well as comparison with previous works [31,38,39]. Fig. 8C presents the Cu LMM Auger signals measured on selected freshly reduced and used ZCuMgAl samples (Z = 0.6, 8.0 and 32.7 wt.% Cu) showing the band positions in kinetic energy units (K.E.). In freshly reduced samples, bands were clearly assigned to Cu° (918.0–919.0 eV), except for the low loading sample 0.6CuMgAl. Contrarily, broader signals in used samples indicated the presence of oxidized species in addition to the Cu° signal; Cu^{2+} was ruled out since no satellite peak was observed in the 2p region (not shown), but an incipient Cu^{1+} signal at ~917 eV was found in samples 8.0CuMgAl (curve (e) and 32.7CuMgAl (curve (f). Thus, in addition to carbon deposition, partial oxidation of the Cu particles is likely to contribute to the overall deactivation process. That is predicted by k_{d3} in Eq. (4).

3.4. Regeneration

After concluding that deactivation is mainly caused by deposition of carbonaceous residues, the possibility of catalyst regeneration by

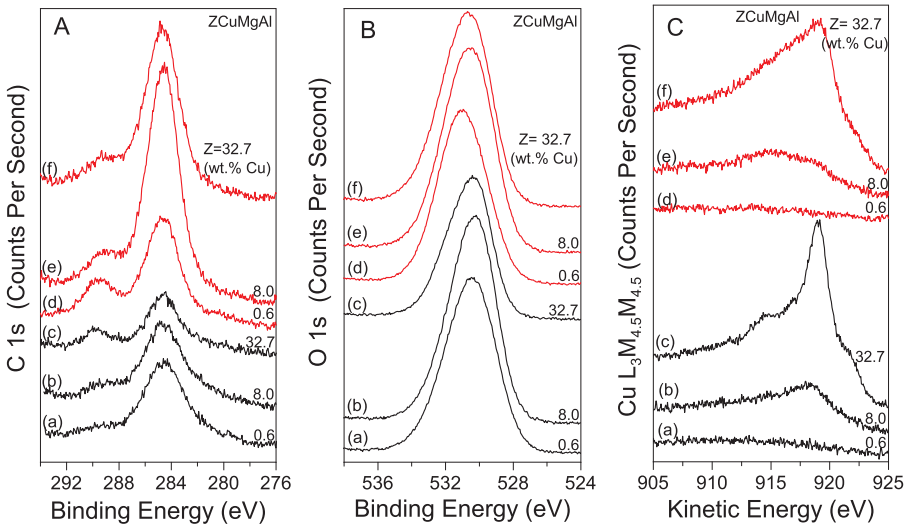

Fig. 8. XPS and Auger spectra of selected ZCuMgAl samples (Z = 0.6, 8.0 and 32.7 wt.% Cu) in the (A) C1s; (B) O1s and (C) Cu LMM regions. (a), (b) and (c): fresh samples after reduction; (d), (e) and (f): after catalytic testing at $X_{C6O_{t=0}}$~ 50%.

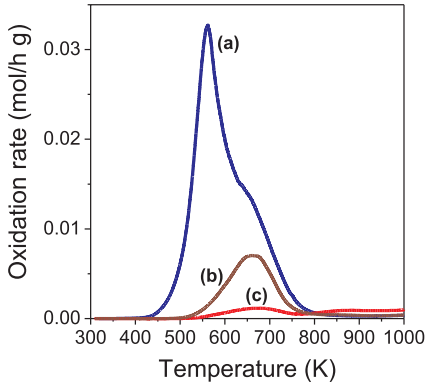

Fig. 9. TPO analysis of used and partially regenerated catalyst 8.0CuMgAl. (a) after catalytic test [W/F^0_{C6OL} = 200 gh/mol; T = 573 K; P = 101.3 kPa; $\overline{P}_{C6OL}$ = 4.1 kPa; N_2 balance]; (b) after regeneration in air at 573 K; (c) after regeneration in air at 673 K.

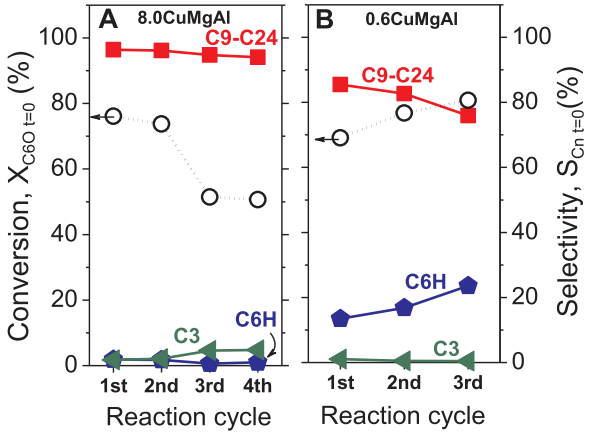

Fig. 10. Conversion and selectivity to main products for fresh (1st cycle) and regenerated catalysts (following cycles). (A) 8.0CuMgAl; (B) 0.6CuMgAl [t = 0; T = 573 K; P = 101.3 kPa; $\overline{P}_{C6OL}$ = 4.1 kPa; N_2 balance].

carbon oxidation was studied. The TPO experiments of Fig. 4 showed that carbon deposits on ZCuMgAl catalysts can be completely removed by oxidation at temperatures close to 750 K using a 2% O_2/N_2 gas mixture. However, to implement the regeneration procedure using conditions similar to those of the TPO experiments, with such a high final temperature, might lead to a substantial sintering of the Cu° particles. Therefore, regeneration using higher oxygen partial pressures is advisable to increase the oxidation kinetics in order to reach complete oxidation at lower temperatures. Consequently, and for practical reasons, the use of air for regeneration purposes was investigated.

In order to find the conditions for catalyst regeneration, one of the most promising samples (8.0CuMgAl) was tested at 573 K and W/F^0_{C6OL} = 200 gh/mol, the other conditions being indicated in Fig. 3; the resulting $X_{C6O_{t=0}}$ was 76%. After the catalytic test, one portion of the used catalyst was analyzed by TPO using a 2%O_2/N_2 gas mixture as oxidant; the carbon content measured by integration of the TPO profile, curve (a) in Fig. 9, was 7.9%. The shape of the TPO curve is similar to those of Fig. 4 obtained at lower conversions, presenting a low temperature peak (l.t.p.) at 556 K and a smaller high temperature peak (h.t.p.) at 617 K.

Two more portions of used catalyst 8.0CuMgAl were oxidized in separate experiments using an air flow of 60 mL/min and i) a ramp rate of 10 K/min up to 573 K; ii) a ramp rate of 10 K/min up to 573 K and then of 5 K/min up to 673 K; in both experiments samples were kept at the final temperature for 2 h. After these oxidation experiments in air, both samples were analyzed by TPO to measure the remaining carbon content, Fig. 9, curves (b) and (c). As can be seen in curve (b), the oxidation in air up to 573 K removed most of the l.t.p. of the carbon deposit and lowered the total carbon content from 7.9% to 1.9%. On the other hand, the treatment in air up to 673 K, curve (c), oxidized most of the carbon residue leading to a final carbon content of 0.4%. Thus, oxidation in air for 2 h at 673 K was chosen as the preferred regeneration procedure. Comparable procedures have been reported by other researchers for the regeneration of copper-based catalysts employed in the dehydrogenation of alcohols [40,41].

To investigate if the regeneration treatment restores the catalytic activity, catalyst 8.0CuMgAl used and regenerated at 673 K was reduced at 573 K in flowing H_2 and submitted to a second catalytic test at 573 K and W/F^0_{C6OL} = 200 gh/mol. Afterwards, the oxidation, reduction and catalytic test cycle was repeated two more times under similar conditions. The results obtained with sample 8.0CuMgAl comparing the four catalytic cycles at t = 0 are presented in Fig. 10A; the regeneration process was successful and in the second cycle the activity, in terms of conversion, was almost completely recovered ($X_{C6O_{t=0}}$ = 71%). However, conversion decreased to 51% in the following cycles.

The surface area of catalyst 8.0CuMgAl after the 4th cycle noticeably dropped (155 m^2/g) compared to the fresh catalyst, which is attributable to a partial destruction of the porous structure during regeneration. The exothermic carbon oxidation probably gives rise to particle temperatures much higher than that of the gas phase, thereby causing the collapse of the porous structure during carbon burning. Thus, a lower accessibility to the active sites accounts for the conversion decay that parallels that of surface area.

The selectivity to C9-C24 products with diesel and jet fuel applications remained above 94% in the four cycles but the yield dropped as a result of the conversion decay over the cycles (65% of the original C9-C24 yield was measured after four cycles). The fact that the product selectivity remains unaffected during the cycles indicates that the chemical nature of the different catalyst active sites and the cooperation between them are not substantially modified by the regeneration procedure. However, a slightly enhanced contribution of C9, C15 and C21 products was observed during recycling, compared to the fresh catalyst. This is ascribed to a change in the copper oxidation state after successive regeneration steps. Cu^{1+} species formed during reaction are more difficult to reduce/oxidize than the $Cu^{2+}/Cu°$ counterparts [42,43]. Thus, during reuse the surface is probably being progressively enriched in Cu^{n+} species (as explained in section 3.3.2) that might perform as Lewis acid centers; on a surface with less available Cu° sites that participate in hydrogenation steps, the reaction pathway would shift toward formation of odd carbon atom number products (C9, C15 and C21), as depicted in Scheme 1 [11].

Regeneration was also attempted with a low Z value catalyst. In a similar fashion, sample 0.6CuMgAl was evaluated following the regeneration/reduction procedure described above. First, this catalyst was tested at 573 K and W/F^0_{C6OL} = 241 gh/mol, the other conditions as in Fig. 3; the resulting $X_{C6O_{t=0}}$ was 69%. Next, the oxidation, reduction and catalytic test cycle was repeated twice and the comparative results of the three cycles at t = 0 are presented in Fig. 10B. The selectivity toward C9-C24 products decreased gradually from 86% to 76% whereas that of the dehydration/hydrogenation products (C6H) concomitantly increased, as well as the conversion. The consequence was that the yield to C9-C24 products was the same during the three cycles, being therefore unaffected by the regeneration/reuse procedure.

The surface area of sample 0.6CuMgAl remained unchanged through the cycles (167 m^2/g after the first use (Table 2) and 156 m^2/g after the 3rd cycle) because the low Cu° content probably restricts the particle temperature evolution during catalytic carbon oxidation, therefore preventing the porous structure from collapsing. The changes in conversion and selectivity are then explained by the incomplete carbon oxidation at 673 K during regeneration procedures. On low Cu loading catalysts, carbon deposits formed on basic sites are difficult to oxidize (Fig. 4 and h.t.p. in Table 2) and therefore, the remaining coke residues would decrease the number of available basic sites for the next

cycle. Thus, the C−C bond forming route would be inhibited to some extent and as a consequence, the reaction pathway would shift to the less demanding formation of C6H with the concomitant conversion increase.

Although reuse of ZCuMgAl samples of high copper loadings (Z ≥ 15 wt.%Cu) was not investigated, regeneration by oxidation of sample 32.7CuMgAl was performed at the conditions described above for the other two samples. CuO crystallite size measurements by XRD using the Scherrer`s equation indicated 71 Å for the fresh sample (other properties in Table 1) and 78 Å after catalytic test at $X_{C6O_{t=0}}$ ~50% (*SA* in Table 2) followed by oxidation. Thus, regeneration of high Z value samples causes no significant changes of the CuO particle size.

In summary, regeneration by oxidation of the carbon deposits in air at 673 K followed by reduction in H_2 at 573 K, might cause loss of either surface area or number of basic sites and partially restores the catalytic performance of ZCuMgAl catalysts.

4. Conclusions

Cu-Mg-Al mixed oxides with copper loadings in the range of 0.3–61.2 wt.% Cu transform 2-hexanol, a model molecule of the primary conversion of sugars, into jet fuel precursors (C9-C24 oxygenates and hydrocarbons) with low oxygen content. The activity and selectivity of these materials and the quality of the resulting products (molecular weight and oxygenate content) depend on the copper loading. The best performances were obtained with 0.6–8.0 wt.% Cu, giving the highest C9-C24 yields at both, t = 0 and the end of the run. The use of high contact times (300–350 g h/mol) favors formation of C9-C24 compounds and decreases the oxygenates/hydrocarbons ratio.

Deactivation of Cu-Mg-Al mixed oxides is mainly caused by carbon deposition and, to a lesser extent, by oxidation of the surface copper species under reaction. Oxygenates (reactants and products) strongly adsorb on the surface and block the active sites causing deactivation. The initial deactivation rate (r_{d0}) measured on Cu-Mg-Al catalysts depends on the catalyst composition and reaction conditions. The fact that on low copper content catalysts r_{d0} decreases with increasing the contact time but that the opposite occurs at high copper loadings, was attributed to deactivation by deposition of the reactant pool on the former and of heavy oxygenates on the latter.

Several oxidation/reduction/catalytic test cycles of used Cu-Mg-Al mixed oxides with 0.6–8.0 wt.% Cu were carried out. Between 65–100% of the original C9-C24 yield was retained after four cycles. However, depending on the catalyst composition, the catalyst reuse is limited by the surface area loss during exothermic oxidation of carbon deposits or by the dropped of the number of available basic sites.

Results presented here highlight the crucial role of the copper content on the catalytic performance of Cu-Mg-Al mixed oxides toward C9-C24 products and on the stability of those materials.

Acknowledgements

Authors thank the Agencia Nacional de Promoción Científica y Tecnológica (ANPCyT), Argentina (grants PICT 1888/10 and PME8-2003), CONICET, Argentina (grant PIP 11220120100503) and Universidad Nacional del Litoral, Santa Fe, Argentina (grant CAID PI 64-103/11) for financial support of this work.

Authors also thank M.F. Mori for the help to process the XPS and Auger spectra.

Appendix A. Supplementary data

Supplementary material related to this article can be found, in the online version, at doi:https://doi.org/10.1016/j.mcat.2018.08.008.

References

[1] D.A. Simonetti, J.A. Dumesic, Catalytic strategies for changing the energy content and achieving C-C coupling in biomass-derived oxygenated hydrocarbons, ChemSusChem 1 (2008) 725–733.
[2] E.R. Sacia, M.H. Deaner, Y. Louie, A.T. Bell, Synthesis of biomass-derived methylcyclopentane as a gasoline additive via aldol condensation/hydrodeoxygenation of 2,5-hexanedione, Green Chem. 17 (2015) 2393–2397.
[3] D.J. Hayes, An examination of biorefining processes, catalysts and challenges, Catal. Today 145 (1-2) (2009) 138–151.
[4] A. Corma, S. Iborra, A. Velty, Chemical routes for the transformation of biomass into chemicals, Chem. Rev. 107 (2007) 2411–2502.
[5] J.Q. Bond, D.M. Alonso, J.A. Dumesic, Catalytic strategies for converting lignocellulosic carbohydrates to fuels and chemicals, in: C.E. Wyman (Ed.), Aqueous Pretreatment of Plant Biomass for Biological and Chemical Conversion to Fuels and Chemicals, John Wiley & Sons, Ltd, UK, 2013, pp. 61–102.
[6] A. Milbrandt, C. Kinchin, R. McCormick, The Feasibility of Producing and Using Biomass-Based Diesel and Jet Fuel in the United States, Technical Report NREL/TP-6A20-58015, (2013).
[7] J.N. Chheda, J.A. Dumesic, An overview of dehydration, aldol-condensation and hydrogenation processes for production of liquid alkanes from biomass-derived carbohydrates, Catal. Today 123 (2007) 59–70.
[8] E.L. Kunkes, D.A. Simonetti, R.M. West, J.C. Serrano-Ruiz, C.A. Gärtner, J.A. Dumesic, Catalytic conversion of biomass to monofunctional hydrocarbons and targeted liquid-fuel classes, Science 322 (2008) 417–421.
[9] E.R. Sacia, M. Balakrishnan, M.H. Deaner, K.A. Goulas, F.D. Toste, A.T. Bell, Highly selective condensation of biomass-derived methyl ketones as a source of aviation fuel, ChemSusChem 8 (2015) 1726–1736.
[10] R.M. West, E.L. Kunkes, D.A. Simonetti, J.A. Dumesic, Catalytic conversion of biomass-derived carbohydrates to fuels and chemicals by formation and upgrading of mono-functional hydrocarbon intermediates, Catal. Today 147 (2009) 115–125.
[11] P.J. Luggren, C.R. Apesteguía, J.I. Di Cosimo, Liquid transportation fuels from biomass-derived oxygenates: gas-phase 2-hexanol upgrading on Cu-based mixed oxides, Appl. Catal. A: Gen. 504 (2015) 256–265.
[12] P.J. Luggren, C.R. Apesteguía, J.I. Di Cosimo, Conversion of biomass-derived 2-hexanol to liquid transportation fuels: study of the reaction mechanism on Cu-Mg-Al mixed oxides, Top. Catal. 59 (2-4) (2016) 196–206.
[13] P.J. Luggren, C.R. Apesteguía, J.I. Di Cosimo, Upgrading of biomass-derived 2-hexanol to liquid transportation fuels on Cu-Mg-Al mixed oxides. Effect of Cu content, Fuel 177 (2016) 28–38.
[14] J.I. Di Cosimo, G. Torres, C.R. Apesteguía, One-step MIBK synthesis: a new process from 2-propanol, J. Catal. 208 (2002) 114–123.
[15] P.A. Torresi, V.K. Díez, P.J. Luggren, J.I. Di Cosimo, Conversion of diols by dehydrogenation and dehydration reactions on silica-supported copper catalysts, Appl. Catal. A: Gen. 458 (2013) 119–129.
[16] S. Sato, R. Takahashi, T. Sodesawa, K. Yuma, Y. Obata, Distinction between surface and bulk oxidation of Cu through N_2O decomposition, J. Catal. 196 (2000) 195–199.
[17] C.J.G. Van Der Grift, A.F.H. Wielers, B.P.J. Joghi, J. Van Beijnum, M. De Boer, M. Versluijs-Helder, J.W. Geus, Effect of the reduction treatment on the structure and reactivity of silica-supported copper particles, J. Catal. 131 (1991) 178–189.
[18] E.L. Kunkes, E.I. Gürbüz, J.A. Dumesic, Vapor-phase C−C coupling reactions of biomass-derived oxygenates over Pd/CeZrOx catalysts, J. Catal. 266 (2009) 236–249.
[19] J.I. Di Cosimo, V.K. Díez, M. Xu, E. Iglesia, C.R. Apesteguía, Structure and surface and catalytic properties of Mg-Al basic oxides, J. Catal. 78 (1998) 499–510.
[20] R.T. Figueiredo, H. Martins Carvalho Andrade, J.L.G. Fierro, Low temperature water gas-shift catalysts, J. Mol. Catal. A: Chem. 318 (2010) 15–20.
[21] G. Torres, C.R. Apesteguía, J.I. Di Cosimo, One-step MIBK synthesis from 2-propanol: catalyst and reaction condition optimization, Appl. Catal. A: Gen. 317 (2007) 161–170.
[22] P. Djinovic, J. Levec, A. Pintar, Effect of structural and acidity/basicity changes of CuO-CeO_2 Catalysts on their activity for water-gas shift reaction, Catal. Today 138 (2008) 222–227.
[23] F. Song, Y. Tan, H. Xie, Q. Zhang, Y. Han, Direct synthesis of dimethyl ether from biomass-derived syngas over Cu–ZnO–Al2O3–ZrO2(x)/γ-Al2O3 bifunctional catalysts: effect of Zr-loading, Fuel Proc. Technol. 126 (2014) 88–94.
[24] M. Xu, M.J.L. Gines, A. Hilmen, B.L. Stephens, E. Iglesia, Isobutanol and methanol synthesis on copper catalysts supported on modified magnesium oxide, J. Catal. 171 (1997) 130–147.
[25] D.A. Monti, A. Baiker, Temperature-programmed reduction. Parametric sensitivity and estimation of kinetic parameters, J. Catal. 83 (1983) 323–335.
[26] J.I. Di Cosimo, C.R. Apesteguía, Study of the catalyst deactivation in the base-catalyzed oligomerization of acetone, J. Mol. Catal. A: Chem. 130 (1998) 177–185.
[27] V.K. Díez, C.R. Apesteguía, J.I. Di Cosimo, Effect of the acid-base properties of Mg-Al mixed oxides on the catalyst deactivation during aldol condensation reactions, Latin Am. Appl. Res. 33 (2) (2003) 79–86.
[28] O. Levenspiel, Chemical Reaction Engineering, 3rd ed., John Wiley and Sons, New York, 1999.
[29] S. Szepe, O. Levenspiel, Chem. Eng. Sci. 23 (1968) 881–894.
[30] J.J. Bravo-Suarez, B. Subramaniam, R.V. Chaudhari, Vapor-phase methanol and ethanol coupling reactions on CuMgAl mixed metal oxides, Appl. Catal. A: Gen. 455 (2013) 234–246.
[31] E. Jobson, A. Baiker, A. Wokaun, J. Mol. Catal. 60 (1990) 399–416.
[32] D. Liu, D. Zemlyanov, T. Wua, R.J. Lobo-Lapidus, J.A. Dumesic, J.T. Miller,

C.L. Marshall, Deactivation mechanistic studies of copper chromite catalyst for selective hydrogenation of 2-furfuraldehyde, J. Catal. 299 (2013) 336–345.
[33] E. Simón, J.M. Rosas, A. Santos, A. Romero, Coke formation in copper catalyst during cyclohexanol dehydrogenation: kinetic deactivation model and catalyst characterization, Chem. Eng. J. 214 (2013) 119–128.
[34] J.F. Moulder, W.F. Stickle, P.E. Sobol, K.D. Bomben, J. Chastain (Ed.), Handbook of X-Ray Photoelectron Spectroscopy, Perkin-Elmer Corporation Physical Electronics Division, Minnesota, 1992.
[35] G.P. Lopez, D.G. Castner, B.D. Ratner, XPS O1s binding energies for polymers containing hydroxyl, ether, ketone and ester groups, Surf. Interface Anal. 17 (1991) 267–272.
[36] Thermo Scientific XPS Elements Table, https://xpssimplified.com/periodictable.php.
[37] G. Moretti, The Wagner plot and the Auger parameter as tools to separate initial- and final-state contributions in X-ray photoemission spectroscopy, Surf. Sci. 618 (2013) 3–11.
[38] M.C. Biesinger, L.W.M. Lau, A.R. Gerson, R.St.C. Smart, Resolving surface chemical states in XPS analysis of first row transition metals, oxides and hydroxides: Sc, Ti, V, Cu and Zn, Appl. Surf. Sci. 257 (2010) 887–898.
[39] Q.-N. Wang, L. Shi, W. Li, W.-C. Li, R. Si, F. Schuth, A.-H. Lu, Cu supported on thin carbon layer coated porous SiO_2 for efficient ethanol dehydrogenation, Catal. Sci. Technol. 8 (2018) 472–479.
[40] E. Simón, J.M. Rosas, A. Santos, A. Romero, Study of the deactivation of copper-based catalysts for dehydrogenation of cyclohexanol to cyclohexanone, Catal. Today 187 (2012) 150–158.
[41] A.J. Marchi, J.L.G. Fierro, J. Santamaria, A. Monzón, Dehydrogenation of isopropylic alcohol on a Cu/SiO2 catalyst: a study of the activity evolution and reactivation of the catalyst, Appl. Catal. A: Gen. 142 (1996) 375–386.
[42] K. Nagase, Y. Zheng, Y. Kodama, J. Kakuta, Dynamic study of the oxidation state of copper in the course of carbon monoxide oxidation over powdered CuO and Cu_2O, J. Catal. 187 (1999) 123–130.
[43] J.Y. Kim, J.A. Rodriguez, J.C. Hanson, A.I. Frenkel, P.L. Lee, Reduction of CuO and Cu_2O with H_2: H embedding and kinetic effects in the formation of suboxides, J. Am. Chem. Soc. 125 (2003) 10684–10692.